Bulletin of the Seismological Society of America, Vol. 97, No. 5, pp. 1621–1631, October 2007, doi: 10.1785/0120050264

Moho Depth and Crustal V_P/V_S Variation in Southern Korea from Teleseismic Receiver Functions: Implication for Tectonic Affinity between the Korean Peninsula and China

by Sung-Joon Chang* and Chang-Eob Baag

Abstract We estimated Moho depths and V_P/V_S ratios of the crust under 21 broadband stations in southern Korea by using a grid search in the crustal thickness–V_P/V_S ratio (H-κ) domain. The Moho depth varies from 25.9 km to 32.5 km, and the V_P/V_S ratio ranges from 1.71 to 1.82 inland. Moho depths in the southernmost area of the Korean Peninsula were estimated shallower than those of the previous results obtained assuming a Poisson solid in the joint analysis of receiver functions and surface-wave dispersion. This southernmost area is roughly in accord with the Yeongnam massif, where relatively high V_P/V_S ratios of 1.78–1.82 are estimated. On the contrary, comparatively low V_P/V_S ratio measurements (1.71–1.76) are generally distributed in the Gyeonggi massif, which is located in the central area of the Korean Peninsula. The major factor for the high V_P/V_S ratios in the Yeongnam massif is thought to be the plagioclase-rich mafic composition of the lower crust rather than partial melting or crustal fluids, because high crustal S-wave velocities are reported in the Yeongnam massif. The mafic composition might have been supplied by the magmatic underplating. From the clearly divided feature of V_P/V_S ratios in southern Korea and the V_P/V_S ratio similarities between southern Korea and China, it seems that the Yeongnam massif might be related to the Sino-Korea craton, whereas the Gyeonggi massif is related to the Yangtze craton.

Introduction

The ratio of a P-wave velocity over an S-wave velocity (V_P/V_S) offers important information on the physical properties of the continental crust. For example, we can guess the general composition of the upper crust with a V_P/V_S ratio because V_P/V_S ratio values are about 1.73 for felsic rocks, whereas the values for mafic rocks tend to be greater than 1.73 (Christensen and Fountain, 1975; Kern, 1982; Tarkov and Vavakin, 1982; Fountain and Christensen, 1989; Christensen, 1996). The V_P/V_S ratios of crustal rocks are mainly controlled by the mineral contents of plagioclase with high Poisson's ratio and silica with low Poisson's ratio. Rocks with silica contents of 55–75% (mafic to felsic) have a reverse relationship between the ratio and the silica contents. On the other hand, the ratio becomes large with increased plagioclase contents for the mafic to ultramafic rocks with silica contents less than 55% (Christensen, 1996). For another example, we can recognize the presence of crustal fluids or partial melting from a high V_P/V_S ratio, because shear-wave velocities diminish more at the presence of fluids within the upper crust than compressional-wave velocities do (Christensen, 1989; Fountain and Christensen, 1989). Therefore, information regarding V_P/V_S ratios could help us to gain a better understanding about the characteristics of crust, and researchers have used V_P/V_S ratios to infer the physical properties of the crust (e.g., Poirier, 1987; Zandt and Ammon, 1995; Zandt *et al.*, 1994, 1995).

To obtain the physical properties of the crust in southern Korea, we estimated the Moho depths and V_P/V_S ratios from teleseismic receiver functions. We expect that the information on V_P/V_S ratios could help us to obtain reasonable inference on the tectonic affinity between southern Korea and China by offering physical properties of the massifs in southern Korea. There have been debates on the tectonic affinity of the two massifs, the Gyeonggi and the Yeongnam massifs, in southern Korea to two cratons, the Sino-Korea and the Yangtze cratons, in China, since it has been proposed that Dabie-Sulu collision belt that separates the Sino-Korea and the Yangtze cratons extends to the Imjingang belt in the middle of the Korean Peninsula (Fig. 1) (Yin and Nie, 1993; Li, 1994; Ernst and Liou, 1995; Chang, 1996; Ree *et al.*, 1996; Chough *et al.*, 2000; Lee *et al.*, 2000). Cluzel *et al.*

*Present address: Department of Earth and Planetary Sciences, Northwestern University, Evanston, Illinois 60208.

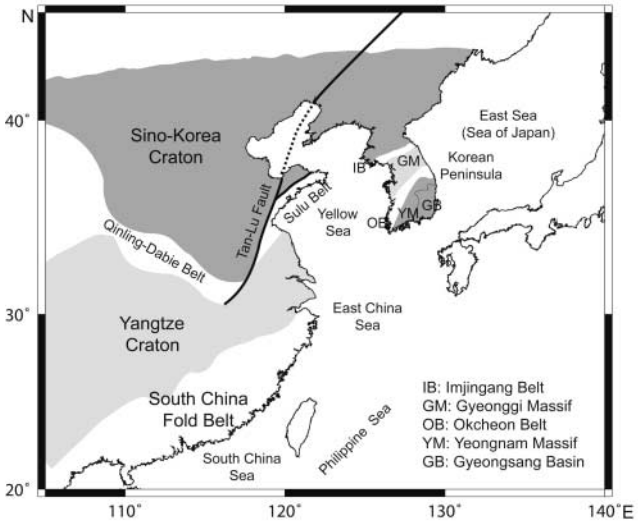

Figure 1. Simplified tectonic map of East Asia. Folded belt areas are illustrated in white, and cratons and massifs are depicted in gray. Faults are represented by thick solid lines.

(1991) and Yin and Nie (1993) suggested that the Gyeonggi massif belongs to the Yangtze craton, whereas the Yeongnam massif belongs to the Sino-Korea craton. However, Cheong *et al.* (2000) and Park *et al.* (2000) suggested that the two Precambrian massifs in southern Korea belong to the Sino-Korea craton. The tectonic correlation between southern Korea and China is still ambiguous because of the lack of petrological and geochronological data for southern Korea (Kwon *et al.*, 2003).

We propose to utilize information about V_P/V_S ratios as an alternative in clarifying the tectonic affinity between southern Korea and China. We estimated V_P/V_S ratios in southern Korea by using a grid search in the H-κ domain suggested by Zhu and Kanamori (2000) where H and κ mean the crustal thickness and the V_P/V_S ratio, respectively. The variations of Moho depths from the grid search are compared with those from computational results obtained assuming a Poisson solid in the joint analysis of receiver functions and surface-wave dispersion (Chang *et al.*, 2004; Chang and Baag, 2005). After presenting the results, we discuss the tectonic affinity between southern Korea and China by using the characteristics of the estimated values.

V_P/V_S Ratio Estimation

The most direct method to estimate the V_P/V_S ratio with seismic data is to utilize travel times of P and S waves from crustal events. However, this method suffers from following two major disadvantages. First, crustal events in general occur in the upper crust, so it is difficult to get information on the V_P/V_S ratio in the lower crust. Second, the estimation for source locations, especially depths of hypocenters, usually gives rise to large errors, depreciating the credibility of the estimated V_P/V_S ratios (Clarke and Silver, 1993). Alternatively, *PmP* and *SmS* waves from the refraction survey can be used to estimate the V_P/V_S ratio (e.g., Holbrook *et al.*, 1992), but it is extremely labor intensive and expensive. Clarke and Silver (1993) estimated V_P/V_S ratios by comparing teleseismic waveforms recorded at permanent or temporary broadband seismographs with synthetic seismograms. They first utilized broadband waveforms including converted waves at the Moho and multiples to estimate V_P/V_S ratios. Zandt and his colleagues (Zandt and Ammon, 1995; Zandt *et al.*, 1994, 1995) removed the need to calculate synthetic seismograms by performing a simple calculation after picking arrival times of converted waves and multiples appearing in receiver functions (Langston, 1979). However, it can be very difficult to identify the phases and measure their arrival times because of background noise, scattering from lateral heterogeneity, and phases from other crustal discontinuities.

Recently, Zhu and Kanamori (2000) proposed a grid search for the V_P/V_S ratio and the crustal thickness where weighted amplitudes of observed radial receiver functions are stacked at predicted arrival times of converted waves at the Moho and multiples in crust. The stacking method is described as

$$s(H, \kappa) = w_1 r(t_1) + w_2 r(t_2) - w_3 r(t_3). \qquad (1)$$

where κ means V_P/V_S ratio, $r(t)$ is the radial receiver function, and t_1, t_2, and t_3 are the predicted arrival times of *Ps*, *PpPms*, and *PpSms* + *PsPms*, respectively. The symbol w_i is the weighting factor for each seismic phase, and $\Sigma w_i = 1$. The maximum value is obtained in the H-κ domain when all three phases are coherently summed in equation (1) with proper H and κ. This method excludes the need to pick the arrival times of seismic phases, so large amounts of teleseismic waveforms can be easily treated. By stacking receiver functions from various azimuths and distances, we can get the average structure, suppressing the effects of lateral structure variation. We applied this method to southern Korea to get the spatial distributions of the Moho depths and V_P/V_S ratios.

Geology and Data

The geology of southern Korea mainly consists of four tectonic provinces: the Imjingang belt, the Gyeonggi massif, the Okcheon belt, and the Yeongnam massif from northwest to southeast (Fig. 1). The Imjingang belt is an east–west-trending fold and thrust zone consisting of metasedimentary rocks and volcaniclastics (Devonian-Carboniferous), underlain unconformably by Proterozoic basement rocks (Chough *et al.*, 2000). Two Precambrian metamorphic massifs, the Gyeonggi and the Yeongnam massifs, separated by the Phanerozoic Okcheon belt consist of high-grade schists and gneisses (Sagong *et al.*, 2005). A Cretaceous sedimentary

basin named the Gyeongsang basin lies on the southeastern part of the Yeongnam massif.

Although the first installation of broadband seismic stations in Korea was done in the mid-1990s, enforcement of installations afterward were occasional until the year 2002 when most of the broadband stations were installed. Therefore, the number of data available for the analysis is limited. We acquired 328 waveforms from 86 teleseismic earthquakes recorded at 21 broadband stations in southern Korea. Earthquakes used for the receiver function estimation are given in previous research (Chang *et al.*, 2004; Chang and Baag, 2005), and additional earthquakes in this study are listed in Table 1. Earthquakes associated with each station are specified in Table 2. We utilized teleseismic earthquakes with various backazimuths occurring in Indonesia, Southwestern Pacific, continental Asia, and Aleutian Islands from 2000 to 2006 with magnitude equal to or larger than 5.8 as shown in Figure 2. Most of the teleseismic events have epicentral distances of 30° to 60°. Because available data are limited as aforementioned, we utilized converted waves at the Moho and multiples by incident *PP* phases as well to estimate receiver functions and raise the reliability of the computational results. Because of low signal-to-noise ratio (SNR) it was more difficult to utilize *PP* waves than *P* waves, and so we used teleseismic events with magnitudes larger than 7 for utilization of *PP* waves to increase SNR. Teleseismic earthquakes for which *PP* waves are utilized are marked by the symbol * in Table 1.

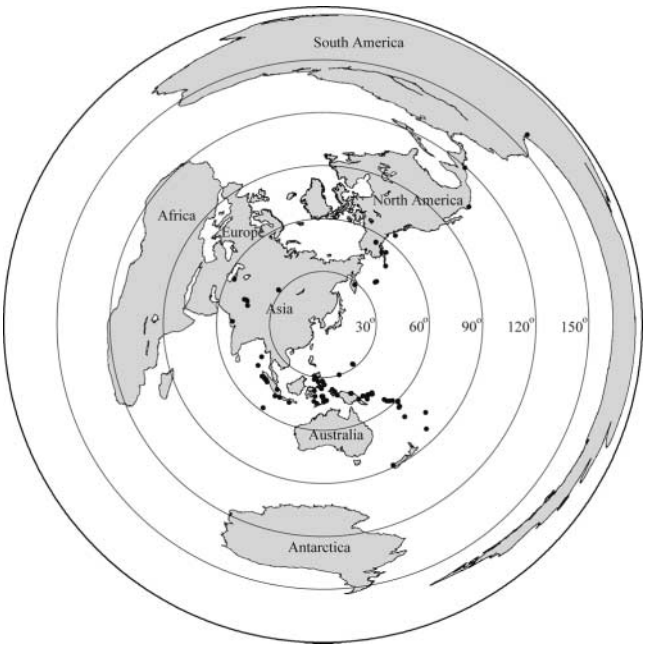

Figure 2. Distribution of teleseismic events for the estimation of the Moho depths and V_P/V_S ratios in southern Korea. Solid circles indicate epicenters of the events. Concentric circles represent angular distances from the center of the seismic network in southern Korea.

Results

Moho depths and V_P/V_S ratio values at 21 stations were estimated based on the method of Zhu and Kanamori (2000). For the estimation of receiver functions, we performed spectral division to deconvolve a vertical component of a teleseismic *P* wave from its horizontal components. The water level value was set to 0.01, and the parameter *a* of the Gaussian filter to 2.5, which gives an effective high-frequency limit of about 0.5 Hz in the *P*-wave data. For the estimation of the arrival times, average crustal *P*-wave velocity of 6.3 km/sec was calculated from the crustal *P*-wave velocities in southern Korea in Chang and Baag (2006). The ray parameters, p, were determined according to epicentral distance of teleseismic events (Ben-Menahem and Singh, 1981), and the weighting factors in equation (1), w_i, were set to be values of 0.7, 0.2, 0.1 for $i = 1, 2, 3$, respectively. Weighted amplitudes of receiver functions at the arrival times were summed at each grid point in the H-κ domain, and the proper crustal thickness and V_P/V_S ratio were obtained from the location of the maximum value of $s(H, \kappa)$. The Moho depth is determined by subtracting the station elevation from the estimated crustal thickness. The locations of broadband stations and the results of the estimation for the Moho depths and V_P/V_S ratios with corresponding standard deviations are shown in Table 3.

The distribution of the 21 Moho depths obtained from the grid search is presented in Figure 3b. The Moho in the southernmost area of the Korean Peninsula is shallower than that estimated from the joint analysis of teleseismic receiver functions and surface-wave dispersions assuming a Poisson's solid of crustal rocks (Chang and Baag, 2005) in Figure 3a. This depth difference is thought to be caused by the different values of the V_P/V_S ratio. We present the amplitude distributions in the H-κ domain of the grid search for all stations in Figure 4 to show the effect of the V_P/V_S ratio variation on the estimation of the Moho depth and the accuracy of the H-κ domain grid search. The darker area with large amplitudes is the place where amplitudes of receiver functions are coherently stacked. As the V_P/V_S ratio gets larger along the trend of darker area, corresponding Moho depth becomes shallower. For example, the estimated V_P/V_S ratio corresponding to the maximum amplitude position in the H-κ plot at the station GKP is larger than that of a Poisson's solid, so the Moho depth becomes shallower than that in the joint-inversion analysis. Therefore, it is essential to consider V_P/V_S ratios in estimating the Moho depth. The stations shown in the two contour maps are a little different from each other, because at each station more data are needed for the grid search that only includes optimized travel-time information than for receiver-function analysis that includes the whole waveforms. Therefore, we had to exclude some stations with small number of data with quality.

The distribution of the Moho depth is in general similar to previous results obtained using gravity data (Kwon and

Table 1
List of Earthquakes Additionally Used for the Calculation of Receiver Functions for the Grid Search in the H-κ Domain

Date (mm/dd/yy)	Time (UT) (hh:mm:ss.s)	Latitude	Longitude	Depth (km)	Magnitude (M_w)	Δ (deg)	BAZ (deg)
05/04/00	04:21:16.2	1.11° S	123.57° E	26.0	7.6	37.5	186
06/04/00	16:28:26.1	4.72° S	102.09° E	33.0	7.9	47.3	215
06/18/00	14:44:13.3	13.80° S	97.45° E	10.0	7.8	57.5	215
08/03/00	01:09:38.9	12.04° S	166.45° E	33.0	6.6	60.7	135
10/04/00	16:58:44.3	15.42° S	166.91° E	23.0	6.8	63.7	137
10/25/00	09:32:23.9	6.55° S	105.63° E	38.0	6.8	47.4	210
12/06/00	17:11:06.4	39.57° N	54.80° E	30.0	7.0	55.8	297
01/09/01	16:49:28.0	14.93° S	167.17° E	103.0	7.0	63.5	136
01/10/01	16:02:44.2	57.08° N	153.21° W	33.0	7.1	54.8	41
01/13/01*	17:33:32.3	13.05° N	88.66° W	60.0	7.7	119.0	42
01/26/01	03:16:40.5	23.42° N	70.23° E	16.0	7.7	50.5	272
06/03/01	02:41:57.1	29.67° S	178.63° W	178.1	7.2	83.1	135
07/28/01	07:32:43.0	59.03° N	155.12° W	131.3	6.6	53.4	39
10/12/01	15:02:16.8	12.69° N	144.98° E	37.0	7.0	28.5	142
10/14/01	01:10:45.6	8.60° S	110.63° E	67.2	5.8	47.5	203
10/31/01	09:10:20.0	5.91° S	150.20° E	33.0	6.9	47.3	148
01/10/02	11:14:56.9	3.21° S	142.43° E	11.0	6.7	42.0	157
02/28/02	01:50:48.9	5.69° S	151.26° E	40.2	6.2	47.5	147
03/03/02	12:08:19.7	36.50° N	70.48° E	225.6	7.4	45.1	288
04/26/02	16:06:07.0	13.09° N	144.62° E	85.7	7.1	28.0	142
06/17/02	21:26:22.9	12.59° S	166.38° E	33.0	6.7	61.1	135
08/14/02	13:12:39.8	7.83° N	136.88° E	10.0	6.3	29.8	161
08/19/02	11:01:01.1	21.70° S	179.51° W	580.0	7.6	76.6	130
09/08/02	18:44:23.7	3.30° S	142.95° E	13.0	7.6	42.2	156
09/13/02	22:28:29.4	13.04° N	93.07° E	21.0	6.5	38.6	242
10/23/02	11:27:19.4	63.51° N	147.91° W	4.2	6.7	55.8	33
11/02/02	01:26:10.7	2.82° N	96.09° E	30.0	7.4	44.2	228
11/03/02	22:12:41.0	63.52° N	147.44° W	4.9	7.9	56.0	33
12/12/02	08:30:42.7	4.79° S	153.28° E	34.0	6.6	47.7	144
01/10/03	13:11:56.9	5.31° S	153.70° E	71.9	6.6	48.3	144
01/20/03	08:43:06.0	10.49° S	160.77° E	33.0	7.3	56.3	139
01/22/03*	02:06:34.6	18.77° N	104.10° W	24.0	7.4	106.5	51
02/19/03	03:32:36.3	53.65° N	164.64° W	19.0	6.6	49.0	47
03/17/03	16:36:17.3	51.27° N	177.98° E	33.0	7.0	38.6	51
03/25/03	02:53:25.0	8.29° S	120.74° E	33.0	6.5	45.0	189
04/27/03	16:03:40.4	20.94° S	169.77° E	77.4	6.3	69.8	138
06/16/03	22:08:02.1	55.49° N	160.00° E	174.8	6.9	29.2	39
07/21/03	13:53:58.4	5.48° S	148.85° E	189.6	6.3	46.3	150
08/21/03	12:12:49.7	45.10° S	167.14° E	28.0	7.2	89.0	153
09/27/03	11:33:25.0	50.04° N	87.81° E	16.0	7.3	31.5	308
10/01/03	01:03:25.2	50.21° N	87.72° E	10.0	6.7	31.6	309
11/17/03	06:43:06.8	51.15° N	178.65° E	33.0	7.8	39.0	51
02/05/04	21:05:02.8	3.62° S	135.54° E	16.6	7.0	40.6	167
02/07/04	02:42:35.2	4.00° S	135.02° E	10.0	7.3	41.0	168
06/28/04	09:49:47.0	54.80° N	134.25° W	20.0	6.8	65.5	39
07/25/04	14:35:19.0	2.43° S	103.98° E	582.1	7.3	44.4	215
10/08/04	08:27:53.5	10.95° S	162.16° E	36.0	6.8	57.5	138
11/09/04	23:58:23.6	11.15° S	163.71° E	13.0	6.9	58.5	137
11/11/04	21:26:41.1	8.15° S	124.87° E	10.0	7.5	44.5	184
02/05/05	12:23:18.9	5.29° N	123.34° E	525.0	7.1	31.2	188
03/02/05	10:42:12.2	6.53° S	129.93° E	201.7	7.1	43.0	176
03/28/05	16:09:36.5	2.09° N	97.11° E	30.0	8.7	44.2	226
03/30/05	16:19:41.1	2.99° N	95.41° E	22.0	6.4	44.5	229
04/16/05	16:38:03.9	1.81° N	97.66° E	31.0	6.4	44.1	225
05/10/05	01:09:05.1	6.23° S	103.14° E	17.0	6.2	48.2	213
05/14/05	05:05:18.4	0.59° N	98.46° E	34.0	6.8	44.6	224
05/19/05	01:54:52.8	1.99° N	97.04° E	30.0	6.9	44.3	226
06/13/05*	22:44:33.9	19.99° S	69.20° W	115.6	7.8	157.3	47
06/14/05	17:10:16.6	51.23° N	179.41° E	51.1	6.8	39.5	51
07/05/05	01:52:02.9	1.82° N	97.08° E	21.0	6.7	44.4	226
07/24/05	15:42:06.2	7.92° N	92.19° E	16.0	7.3	42.8	237
09/09/05	07:26:43.7	4.54° S	153.47° E	90.0	7.7	47.6	143
10/08/05	03:50:40.8	34.54° N	73.59° E	26.0	7.6	43.3	284
01/27/06	16:58:53.6	5.47° S	128.13° E	397.0	7.6	41.7	179

The primary catalog of earthquakes is given in Chang *et al.* (2004) and Chang and Baag (2005). For the events marked by the symbol *, converted waves at the Moho and multiples by incident *PP* phases are utilized to estimate receiver functions.

Yang, 1985; Choi *et al.*, 1993; Choi and Shin, 1996) which show deep Moho depths in the inland area and shallow Moho depths in the coastal area. However, there are deviations of Moho depths beneath the Gyeongsang basin; the Moho depths under the Gyeongsang basin from our results are deeper than those beneath nearby regions, whereas the Moho depths from previous results are shallower. Moreover, this discrepancy can be found in comparison of our results with the two-dimensional travel-time inversion results (Cho *et al.*, 2006) from the seismic-refraction survey. This phenomenon is thought to be caused by the magmatic underplating under this region which is discussed in detail later. The gravity data do not have the resolving power to discern the lowermost layered crustal structure formed by the magmatic underplating and the upper mantle. The travel-time data from near-surface blasts utilized in the tomographic inversion is not complete one, because the acquisition of the data set from the planned shot in the Gyeongsang basin was not possible and the two other shots were far outside of the basin (Cho *et al.*, 2006). In addition, phases from the structure by the magmatic underplating could not be the first arrivals all the time and have small amplitudes due to low-velocity contrast between the lowermost crust of the magmatic underplating and the upper mantle. Thus it was difficult to pick up clear phases from the structure by the magmatic underplating. In conclusion, previous results might be distorted because of the incompleteness of data and difficulty in phase picking, so the structure by the magmatic underplating was not recognized. On the contrary, teleseismic waveforms used in receiver functions include information about the magmatic underplating, because teleseismic waves impinge on the Moho from the mantle. For example, there are two peaks at depths of 28.5 km and 32.5 km, respectively, as seen in the amplitude distribution at station GKP in Figure 4. The shallower depth might mean the top of the layered structure by the magmatic underplating, and the deeper one could indicate the bottom of it. The thickness of 4 km for the layer is consistent with the high-velocity zone with 5 km thickness under station GKP that was found in the receiver-function analysis (Chang and Baag, 2005).

The distribution of 19 V_P/V_S ratios is presented in Figure 5. The most remarkable feature is that high V_P/V_S ratios are concentrated in the southernmost area of the Korean Peninsula that is approximately in accord with the Yeongnam massif. On the other hand, lower values around 1.71–1.76

Table 2
Earthquakes Associated with Each Seismic Station in Estimation of Receiver Functions

Station	Earthquakes for Receiver Function Estimation (mm/dd/yy)
BGD	09/20/02, 10/10/02, 01/10/03, 04/27/03, 05/05/03b, 05/26/03a, 07/21/03, 08/21/03, 10/01/03, 11/17/03, 07/25/04, 03/02/05, 03/30/05, 04/16/05, 06/13/05, 06/14/05, 07/05/05, 07/24/05, 10/08/05, 01/27/06
BRD	03/03/02, 03/05/02, 04/26/02, 09/20/02, 10/10/02, 03/14/03, 03/17/03, 05/05/03a, 05/26/03a, 05/26/03b, 06/16/03, 11/11/04, 06/13/05, 06/14/05, 10/08/05, 01/27/06
BUS	08/19/02, 10/10/02, 11/03/02, 01/22/03, 05/26/03a, 11/17/03, 06/28/04, 02/05/05, 03/02/05, 06/13/05, 06/14/05, 07/05/05, 07/24/05
CHC	03/25/02, 09/20/02, 10/10/02, 11/03/02, 01/22/03, 02/19/03, 03/17/03, 05/05/03a, 05/26/03a, 05/26/03b, 09/27/03, 10/01/03, 03/02/05, 06/13/05
CHJ	02/05/02, 02/28/02, 09/08/02, 10/23/02, 01/22/03, 02/19/03, 05/05/03a, 05/26/03b, 07/21/03, 08/21/03, 09/27/03, 02/05/05, 06/13/05, 06/14/05, 09/09/05
CHNB	01/26/01, 03/19/01, 10/12/01, 01/10/02, 02/05/02, 03/05/02, 08/14/02, 09/08/02, 10/10/02, 01/22/03, 03/17/03, 05/05/03a, 06/28/04, 11/11/04, 06/13/05, 06/14/05
DAG	03/03/02, 10/10/02, 01/22/03, 05/26/03a, 08/21/03, 09/27/03, 11/17/03, 06/13/05, 06/14/05, 07/24/05
DGY	09/20/02, 10/10/02, 11/03/02, 01/20/03, 01/22/03, 02/19/03, 09/27/03, 09/09/05, 01/27/06
GKP	03/03/00, 04/03/00, 05/04/00, 06/14/00, 06/18/00, 07/16/00, 06/05/01, 10/12/01, 10/19/01, 10/31/01, 02/05/02, 03/03/02, 03/05/02, 10/10/02, 11/02/02, 11/03/02, 01/22/03, 05/05/03a, 05/26/03a, 05/26/03b, 08/21/03, 11/09/04, 04/16/05, 05/19/05, 06/13/05, 07/05/05, 07/24/05, 09/09/05, 10/08/05
GSU	06/03/01, 10/31/01, 01/10/02, 06/17/02, 09/08/02, 11/02/02, 01/10/03, 02/19/03, 03/17/03, 05/05/03a, 05/26/03b, 07/21/03, 10/08/04, 04/16/05, 05/14/05
HDB	12/06/00, 01/26/01, 02/24/01, 06/03/01, 10/19/01, 11/20/01, 03/03/02, 03/05/02, 06/17/02, 11/09/04, 11/11/04, 04/16/05, 05/14/05, 05/19/05, 10/08/05, 01/27/06
HKU	04/26/02, 09/08/02, 09/13/02, 10/10/02, 11/02/02, 10/08/04, 05/14/05, 07/05/05, 09/09/05, 05/05/03a, 06/13/05, 10/08/05
HSB	05/05/03a, 05/05/03b, 05/26/03a, 07/21/03, 11/17/03, 02/05/04, 10/08/04, 05/10/05, 05/19/05, 10/08/05, 07/05/05
INCN	11/16/00, 11/18/00, 06/05/01, 10/19/01, 04/26/02, 10/10/02, 11/02/02, 01/20/03, 09/27/03, 11/17/03, 10/08/04, 07/24/05,
KWJ	01/13/01, 01/26/01, 10/14/01, 11/23/01, 03/25/02, 09/20/02, 11/03/02, 01/22/03, 02/19/03, 05/26/03a, 09/27/03, 11/17/03, 02/05/04, 03/28/05, 06/13/05, 07/24/05, 10/08/05, 01/27/06
PUS	06/18/00, 08/07/00, 08/28/00, 10/25/00, 12/06/00, 01/10/01, 07/28/01, 10/19/01
SES	01/13/01, 01/26/01, 03/19/01, 06/05/01, 07/28/01, 10/14/01, 02/05/02, 03/25/02, 01/22/03, 07/21/03, 09/27/03, 11/17/03, 06/28/04, 07/25/04, 03/02/05, 06/14/05, 07/24/05, 01/27/06,
SNU	06/14/00, 08/03/00, 10/04/00, 11/16/00, 11/18/00, 12/06/00, 01/26/01, 03/19/01, 06/03/01, 06/05/01, 10/19/01, 10/31/01, 03/03/02, 06/17/02, 01/10/03, 01/22/03, 03/17/03, 05/05/03a, 05/05/03b, 05/26/03a, 09/27/03, 11/17/03, 02/05/04
TJN	03/03/00, 04/03/00, 06/14/00, 06/18/00, 08/07/00, 10/04/00, 10/25/00, 11/16/00, 11/18/00, 01/10/01, 01/26/01, 02/24/01, 06/03/01, 10/12/01, 10/19/01, 10/31/01, 03/03/02, 06/17/02, 09/20/02, 10/10/02, 12/12/02, 01/22/03, 05/05/03a, 05/05/03b, 05/26/03a, 10/01/03, 02/05/04
ULJ	01/13/01, 10/19/01, 12/23/01, 09/20/02, 01/22/03, 05/26/03a, 07/21/03, 09/27/03, 10/01/03, 11/17/03, 02/05/04, 07/25/04, 10/08/04, 06/13/05, 07/05/05, 09/09/05, 01/27/06
ULL	06/18/00, 11/16/00, 01/09/01, 01/13/01, 01/26/01, 03/03/02, 01/22/03, 08/21/03, 11/17/03
China Digital Seismograph Network	
BJT	06/04/00, 06/18/00, 12/06/00, 01/26/01, 01/10/02, 04/26/02, 09/08/02, 02/07/04, 11/09/04, 03/30/05, 04/16/05, 05/14/05, 05/19/05
SSE	08/28/00, 10/25/00, 12/06/00, 01/10/01, 01/26/01, 03/03/02, 09/08/02, 02/19/03, 03/17/03, 03/25/03, 10/01/03, 02/05/04, 05/10/05, 06/14/05, 10/08/05

For the information of earthquakes, refer to Table 1 of this article, Table 1 in Chang *et al.* (2004), and Table 2 in Chang and Baag (2005).

of the ratio were estimated at stations in the Gyeonggi massif located in the central part of the Korean Peninsula. We have a discussion regarding reasons for the concentration of V_P/V_S ratios and correlations between geologic areas and V_P/V_S ratios in the next section.

Discussion

The most remarkable feature in the spatial distribution of V_P/V_S ratios is that relatively high V_P/V_S ratio values are concentrated in the southernmost area of the Korean Peninsula, whereas the ratio values in the central area (northern part of the study area) are comparatively low. In comparison with the tectonic map in Figure 1, this feature of concentration of V_P/V_S ratios is approximately in accord with two geologic massifs in Korea; that is, high V_P/V_S ratio values are approximately distributed in the Yeongnam massif, whereas low V_P/V_S ratio values are distributed in the Gyeonggi massif.

We first try to infer reasons for the high V_P/V_S ratios in the Yeongnam massif. Two reasons for high V_P/V_S ratios could be possible: crustal fluids and the plagioclase-rich mafic composition of the lower crust. We can tell whether the existence of crustal fluids can be the reason for the high V_P/V_S ratios based on the characteristics of crustal fluids, because the fluid contents in the crust decreases *S*-wave velocities. Looking at the distribution of average crustal *P*-wave velocities in southern Korea shown in Figure 11 of Chang and Baag (2005), which were obtained from receiver-function analysis assuming a Poisson's solid, we can notice

Table 3
Locations of Broadband Stations in Southern Korea and the Estimation Results of the Moho Depths and V_P/V_S Ratios

Station	Longitude (° N)	Latitude (° E)	Elevation (m)	N	Moho Depth (km)	V_P/V_S
BGD	126.5575	34.1569	5.7	20	32.5 ± 2.9	1.78 ± 0.03
BRD	124.7160	37.9743	51.2	16	28.9 ± 2.4	1.81 ± 0.03
BUS	129.1125	35.2487	91.0	13	30.9 ± 3.8	1.79 ± 0.07
CHC	127.8145	37.7775	245.0	14	30.8 ± 3.7	1.71 ± 0.06
CHJ	127.9748	36.8730	227.0	15	32.3 ± 2.1	1.72 ± 0.04
CHNB	127.1185	38.2685	193.3	16	28.8 ± 2.8	1.72 ± 0.06
DAG	128.8970	35.7685	262.0	10	30.7 ± 3.0	1.78 ± 0.05
DGY	128.6742	37.6904	791.0	9	31.2 ± 4.8	1.73 ± 0.05
GKP	128.6083	35.8863	46.5	29	32.5 ± 2.5	1.79 ± 0.05
GSU	128.0991	35.1521	−12.1	15	31.0 ± 4.1	1.82 ± 0.05
HDB	129.4012	35.7307	84.7	16	25.9 ± 4.2	1.81 ± 0.04
HKU	127.3602	36.6102	67.0	12	31.4 ± 2.4	1.74 ± 0.03
HSB	126.6380	36.5525	−7.5	11	30.0 ± 3.1	1.74 ± 0.03
INCN	126.6333	37.4833	420.0	12	29.1 ± 3.6	1.75 ± 0.07
KWJ	126.9910	35.1599	213.0	18	32.3 ± 2.6	1.78 ± 0.04
PUS	129.0338	35.1010	69.2	8	30.9 ± 4.6	–
SES	126.4531	36.7893	99.1	18	29.9 ± 2.0	1.72 ± 0.04
SNU	126.9566	37.4509	161.1	23	28.3 ± 3.1	1.76 ± 0.04
TJN	127.3638	36.3775	52.0	27	30.4 ± 1.1	1.77 ± 0.02
ULJ	129.4084	36.7021	77.1	17	26.4 ± 2.3	1.82 ± 0.02
ULL	130.9008	37.4736	218.3	9	13.3 ± 2.0	–

The minus values in elevation indicate depths below the sea level in the borehole and N means the number of teleseismic events used for the estimation.

that average crustal shear-wave velocities in the Yeongnam massif are higher than those in nearby regions. The Rayleigh-wave phase velocities for 10 and 15 sec, which are sensitive to the shear-wave velocity in the lower crust, are higher in the Yeongnam massif than those in the Gyeonggi massif (Chang and Baag, 2005). Moreover, in recent research for the estimation of one-dimensional average crustal velocity model in southern Korea (Chang and Baag, 2006), observed long-period seismic phases from a local earthquake that occurred in the southeastern part of the Korean Peninsula arrive prior to those of synthetic ones based on the one-dimensional velocity model in southernmost area of the Peninsula. This observation shows that average crustal shear-wave velocity in the southernmost area is higher than that in nearby regions. Therefore, it is strongly suggested that the high V_P/V_S ratio values result from the mafic composition under this area rather than crustal fluid or partial melting.

This assumption of the presence of mafic composition in the Yeongnam massif is supported by a few researchers. Cho *et al.* (2004) discovered a high-velocity structure in the lower crust under the southeastern Korean margin, the eastern side of the Yeongnam massif, from a tomographic inversion. They interpreted the structure as the magmatic underplating by comparing the observed magnetic anomaly with synthetics. Chang and Baag (2005) observed a high-velocity zone of 7.3–7.5 km/sec with a 5-km thickness just above the Moho under station GKP from receiver-function

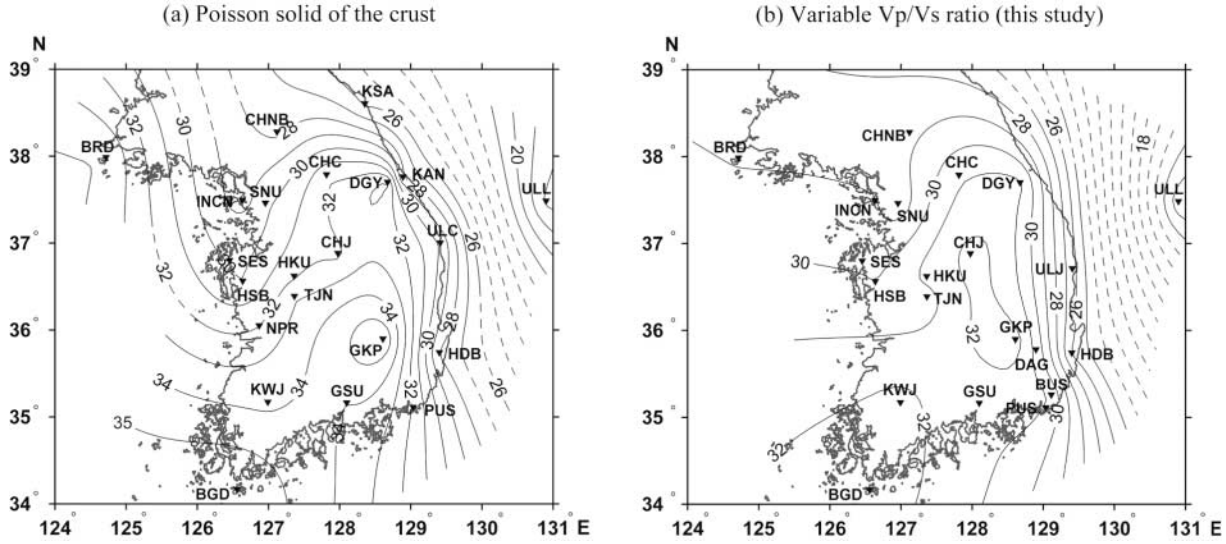

Figure 3. Comparison of Moho depth distributions based on two methods. (a) Distribution of the Moho depth in southern Korea from the joint analysis of teleseismic receiver functions and surface-wave dispersion assuming Poisson's solid of the crust (Chang and Baag, 2005) and (b) distribution of Moho depth in southern Korea obtained from the grid search in the H-κ domain assuming variable V_P/V_S ratio in this study. Filled inverse triangles indicate locations of stations for which station names are assigned. Contours in kilometers are drawn by the interpolation of estimated values at stations. Dashed lines imply uncertain contours caused by scarce distribution of stations.

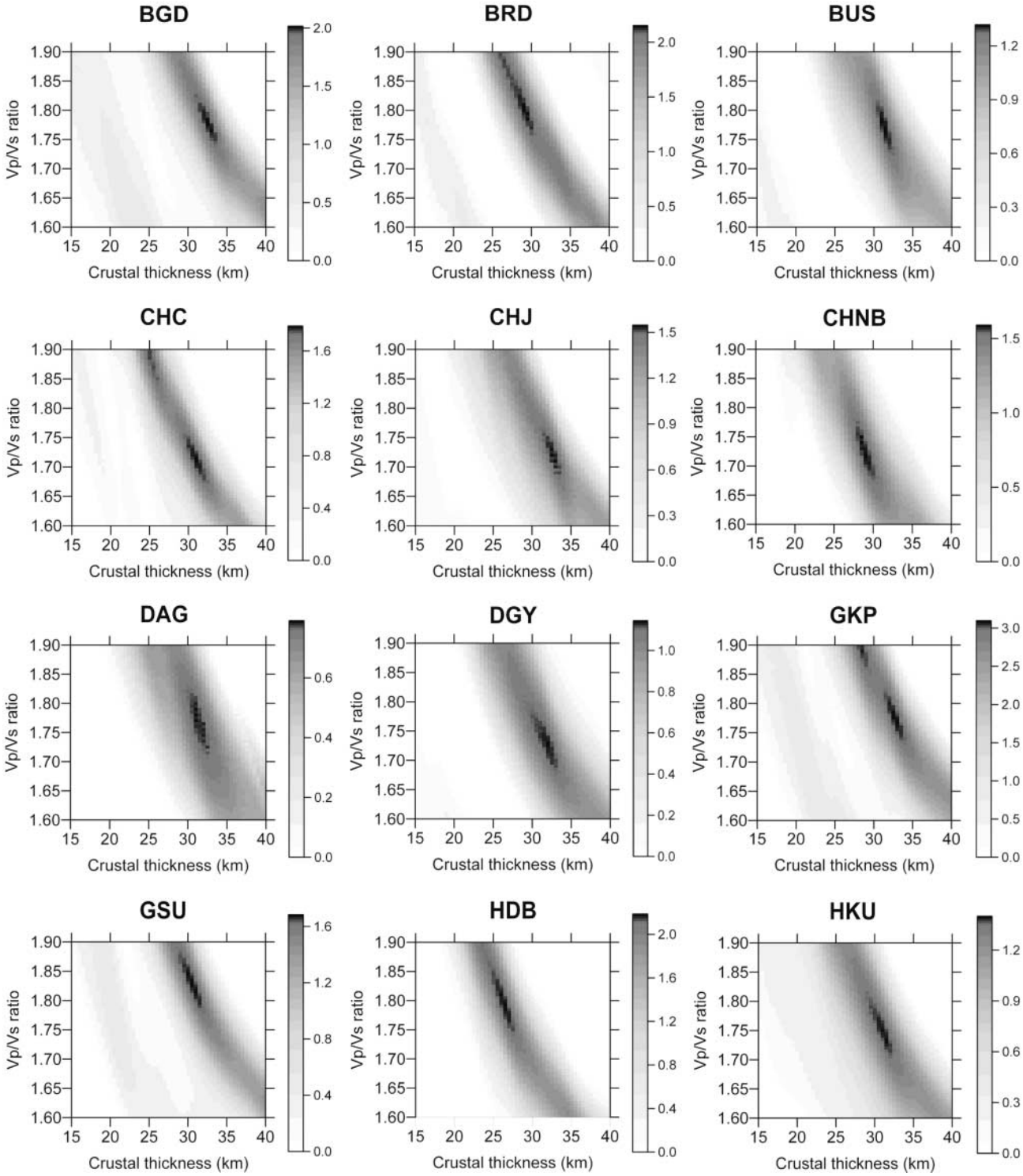

Figure 4. Amplitude distributions in the H-κ domain of the grid search at all the stations. The darker grids mean the area where amplitudes of the three converted seismic phases are coherently stacked. Solutions with negative sum are displayed in white. V_P and V_S represent average velocities in the crust of the P and S waves, respectively. Amplitude distributions at Chinese stations (BJT and SSE) are placed at the end.

(*continued*)

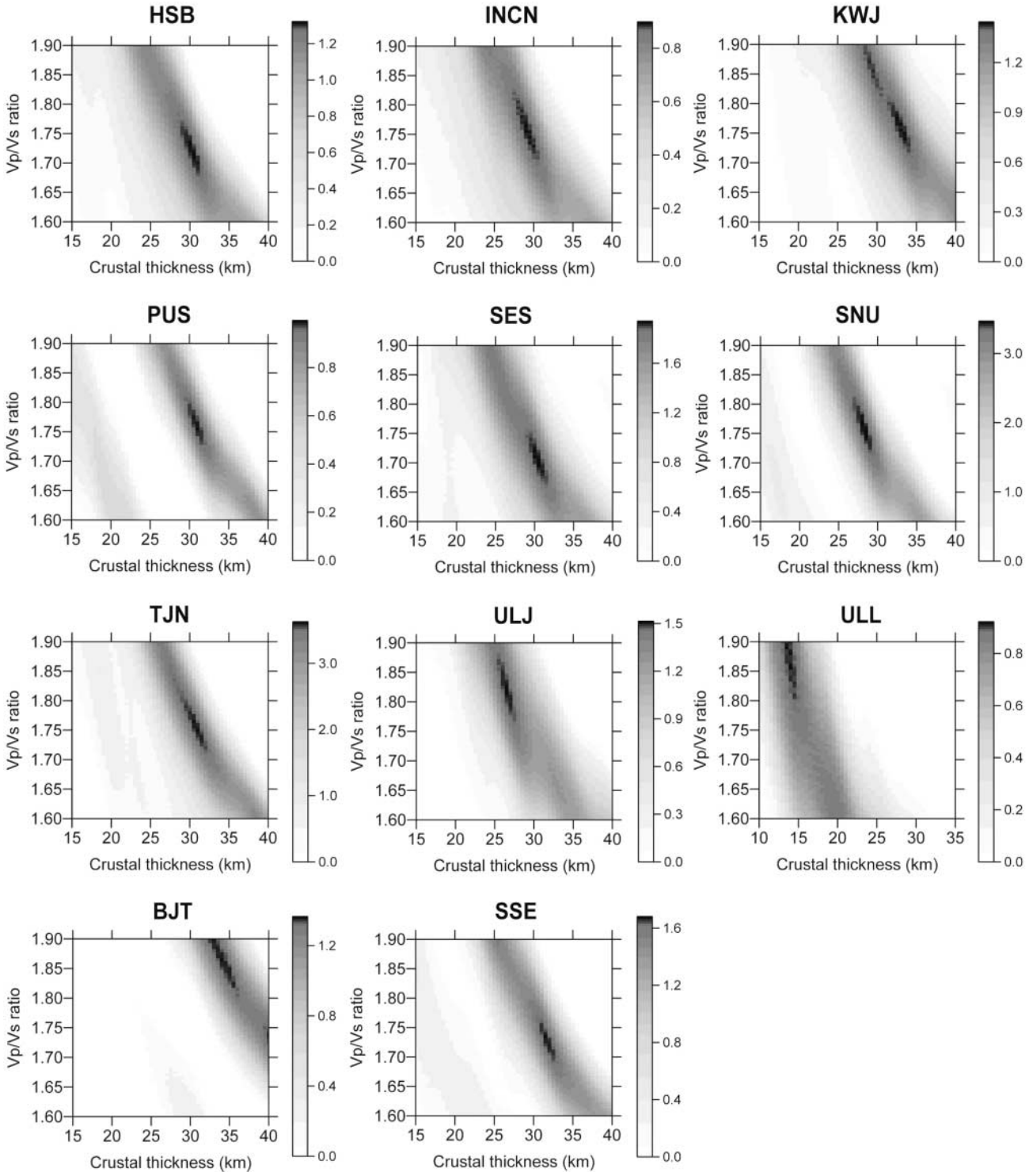

Figure 4. Continued.

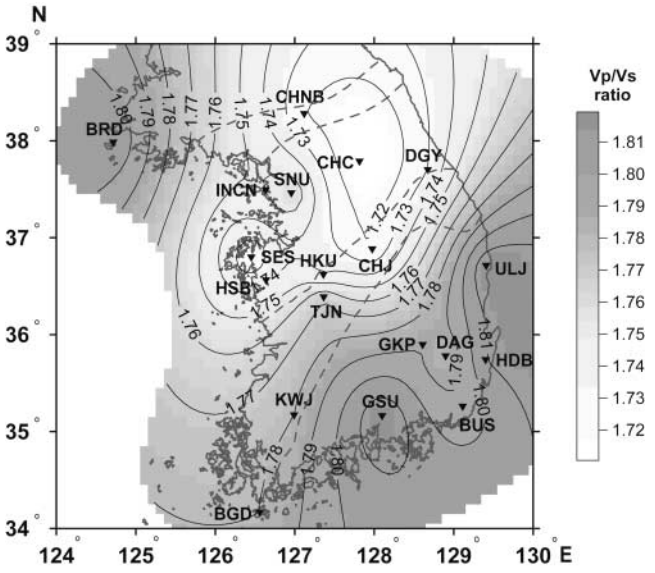

Figure 5. Distribution of V_P/V_S ratio in southern Korea estimated by the grid search in the H-κ domain. V_P and V_S represent average velocities in the crust of the P and S waves, respectively. Dashed lines depict boundaries of tectonic areas as shown in Figure 1.

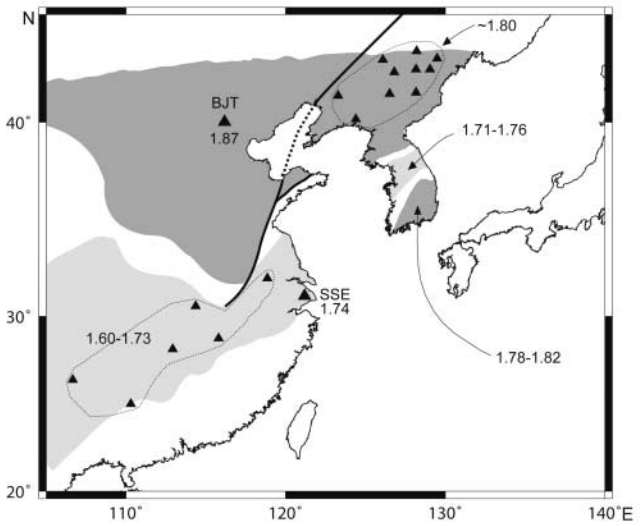

Figure 6. Simplified map showing the distribution of V_P/V_S ratios estimated in this study and those from previous studies. Descriptions on tectonic and geographic locations are given in Figure 1. The V_P/V_S ratio values 1.71–1.76 of the Gyeonggi massif, 1.78–1.82 of the Yeongnam massif, 1.87 at BJT in the Sino-Korea craton, and 1.74 at SSE in the Yangtze craton are obtained in this study. The values around 1.80 in the northeastern Sino-Korea craton (Hetland *et al.*, 2004) and values 1.60–1.73 in the Yangtze craton (Chen *et al.*, 2006) are also shown to be compared. High values (1.78–1.82) in the ratio in the Yeongnam massif are comparable to those of the Sino-Korea craton and low values (1.71–1.76) in the Gyeonggi massif are to those of the Yangtze craton. Therefore, this fact supports the hypothesis that the Gyeonggi massif has tectonic affinity to the Yangtze craton, and the Yeongnam massif has affinity to the Sino-Korea craton.

analysis and guessed that the high-velocity zone is related to the magmatic underplating, which is in accordance with the opinion of Cho *et al.* (2004). The estimated Moho depth around GKP is consistent with that from Kim and Lee (2001).

The differentiated feature of V_P/V_S ratios in the two massifs in southern Korea is similar to the structural feature of the tectonic model suggested by Cluzel *et al.* (1991) and Yin and Nie (1993). From the characteristics of V_P/V_S ratio distribution, it seems to be possible that the two massifs in southern Korea might have collided after a magmatic activity in the Yeongnam massif. If both of the massifs in southern Korea might not belong to the same craton in China, there would be similar systematic difference in V_P/V_S ratios between the two cratons. We estimated V_P/V_S ratios at two stations in China to investigate the presence of the similar difference of V_P/V_S ratios in the two cratons based on the method of Zhu and Kanamori (2000) with data from teleseismic events occurring from 2000 to 2005. The locations of the stations and the estimation results of the Moho depths and V_P/V_S ratios are presented in Figure 6 and Table 4. Earthquakes associated with each station are listed in Table 2.

The ratio value 1.87 at station BJT in the Sino-Korea craton is larger than the value 1.74 at station SSE in the Yangtze craton. Additionally, V_P/V_S ratios estimated at 19 portable broadband stations in the northeastern Sino-Korea craton are about 1.80 on average (Hetland *et al.*, 2004). The high V_P/V_S ratios might have been caused by the partial melt in the volcanic area, but they concluded that it might not be present in large amounts after comparing their results with those of Owens and Zandt (1997), who detected V_P/V_S ratios of 1.91–1.99 in the lower crust of northern Tibet and proposed the presence of partial melt. Therefore, it is more possible that high V_P/V_S ratios in Changbaishan volcanic area originated from the mafic composition. On the other hand, recent research (Chen *et al.*, 2006) for V_P/V_S ratios in southern China using the method of Zhu and Kanamori (2000)

Table 4

Locations of Broadband Stations and the Estimation Results of the Moho Depths and V_P/V_S Ratios in the New China Digital Seismograph Network

Station	Longitude (° N)	Latitude (° E)	Elevation (m)	N*	Moho Depth (km)	V_P/V_S
The Sino-Korea Craton						
BJT	116.17	40.02	197.0	13	33.8 ± 2.9	1.87 ± 0.05
The Yangtze Craton						
SSE	121.19	31.10	15.0	15	31.5 ± 2.4	1.74 ± 0.03

*N means the number of teleseismic events used for the estimation.

revealed that all the V_P/V_S ratios for crust at six stations in the Yangtze craton are under 1.73. We summarize V_P/V_S ratios in this study and from the literature in Figure 6. We mark locations of only 10 stations with more than or equal to 5 receiver functions, each among those given by Hetland *et al.* (2004) in Figure 6, assuming the results with less than 5 receiver functions may be less reliable.

From the V_P/V_S ratio similarity, it could be inferred that the Yeongnam massif might be tectonically related to the Sino-Korea craton, whereas the Gyeonggi massif is related to the Yangtze craton. Another interpretation for the separation of V_P/V_S ratios is that the magmatic underplating might have occurred when the Gyeongsang basin was formed by the subduction of the Izanagi Plate in the early Cretaceous (Chun and Chough, 1992; Maruyama *et al.*, 1997; Chang and Baag, 2005). If the second assumption is correct, V_P/V_S ratio differentiation in southern Korea results from the magmatic activity in Cretaceous; therefore, it could not offer any clue about the tectnonic relationship between southern Korea and China during Permian to Triassic when the Sino-Korea and Yangtze cratons are thought to have collided. However, relatively high V_P/V_S ratios are widely distributed even at places outside of the Gyeongsang basin, so we think the first assumption might be more reasonable. More investigation on V_P/V_S ratios in southern Korea and China is needed to ascertain our inference on the tectonic affinity between southern Korea and China. In conclusion, V_P/V_S ratios may supply an alternative clue for tectonic affinity when petrological and geochronological data are limited.

Conclusions

We presented the distribution of the Moho depths and V_P/V_S ratios in southern Korea using the grid search in the H-κ domain suggested by Zhu and Kanamori (2000). The estimated 21 Moho depths distribute from 25.9 km to 32.5 km, and the depths under the Yeongnam massif are shallower than those in the previous results obtained assuming a Poissons solid in the joint analysis of receiver functions and surface-wave dispersion. This feature is caused by high V_P/V_S ratios of 1.78–1.82 in the Yeongnam massif. On the other hand, V_P/V_S ratio values in the Gyeonggi massif located in central Korea are relatively low, showing values of 1.71–1.76. The concentration of high V_P/V_S ratio values in the Yeongnam massif might be caused by the plagioclase-rich mafic composition of the lower crust, because high crustal *S*-wave velocities and Rayleigh-wave phase velocities observed in this area exclude the possibility of crustal fluids or partial melting as a possible reason for the high V_P/V_S ratios. We think the mafic composition might have been generated by the magmatic underplating based on researches of Cho *et al.* (2004) and Chang and Baag (2005). Based on clearly distinct V_P/V_S ratios in the two massifs, we could imply that both of the two massifs in southern Korea might not belong to the same craton in China. To investigate the V_P/V_S ratio similarity between southern Korea and China, we estimated V_P/V_S ratios at two stations in China and collected V_P/V_S ratio data in China. We found that the similarity exists in such a way that the Yeongnam massif is tectonically related to the Sino-Korea craton, whereas the Gyeonggi massif is related to the Yangtze craton. More investigation on V_P/V_S ratios in southern Korea and China is needed to ascertain this inference. We conclude that the estimation of V_P/V_S ratio might offer qualitative clues in finding the tectonic difference of adjacent massifs.

Acknowledgments

This work was funded by the Korea Meteorological Administration Research and Development Program Grant CATER 2006-5205. We thank Korea Institute of Geoscience and Mineral Resources (KIGAM), Korea Institute of Nuclear Safety (KINS), Korea Meteorological Administration (KMA), and Data Management Center (DMC) of the Incorporated Research Institutions for Seismology (IRIS) for providing their broadband data.

References

Ben-Menahem, A., and S. J. Singh (1981). *Seismic Waves and Sources*, Springer-Verlag, New York, 482–491.

Chang, E. Z. (1996). Collision orgeny between North and South China and its eastern extension in the Korean Peninsula, *J. SE Asian Earth Sci.* **13,** 267–277.

Chang, S.-J., and C.-E. Baag (2005). Crustal structure in southern Korea from joint analysis of teleseismic receiver functions and surface wave dispersion, *Bull. Seism. Soc. Am.* **95,** 1516–1534.

Chang, S.-J., and C.-E. Baag (2006). Crustal structure in southern Korea from joint analysis of regional broadband waveforms and travel times, *Bull. Seism. Soc. Am.* **96,** 856–870.

Chang, S.-J., C.-E. Baag, and C. A. Langston (2004). Joint analysis of teleseismic receiver functions and surface wave dispersion using the genetic algorithm, *Bull. Seism. Soc. Am.* **94,** 691–704.

Chen, Y., H. Tkalcic, R. Liu, Z. Huang, W. Chan, and L. Sun (2006). Comprehensive receiver function analyses for southeastern China, *EOS* **87,** no. 46, S43B-1392.

Cheong, C. S., S.-T. Kwon, and K.-H. Park (2000). Pb and Nd isotopic constraints on Paleoproterozoic crustal evolution of the northeastern Yeongnam Massif, South Korea, *Precambrian Res.* **102,** 207–220.

Cho, H.-M., C.-E. Baag, J. M. Lee, W. M. Moon, H. Jung, K. Y. Kim, and I. Asudeh (2006). Crustal velocity structure across the southern Korean Peninsula from seismic refraction survey, *Geophys. Res. Lett.* **33,** L06307, doi 10.1029/2005GL025145.

Cho, H.-M., H.-J. Kim, H.-T. Jou, J.-K. Hong, and C.-E. Baag (2004). Transition from rifted continental to oceanic crust at the southeastern Korean margin in the East Sea (Japan Sea), *Geophys. Res. Lett.* **31,** L07606, doi 10.1029/2003GL019107.

Choi, K.-S., and Y.-H. Shin (1996). Isostasy in and around the Korean Peninsula by analyzing gravity and topography data, *J. Geol. Soc. Korea* **32,** 407–420 (in Korean).

Choi, K.-S., Y.-S. Kong, and H.-K. Lee (1993). A study on the crustal structure in and around the Korean Peninsula by analyzing gravity data, *J. Korean Earth Sci. Soc.* **14,** 225–230.

Chough, S. K., S.-T. Kwon, J.-H. Ree, and D. K. Choi (2000). Tectonic and sedimentary evolution of the Korean peninsula: a review and new view, *Earth Sci. Rev.* **52,** 175–235.

Christensen, N. I. (1989). Pore pressure, seismic velocities, and crustal structure, in *Geophysical Framework of the Continental United States*, L. C. Pakiser and W. D. Mooney (Editors), Geol. Soc. Am. Memoir Vol. 172, 783–798.

Christensen, N. I. (1996). Poisson's ratio and crustal seismology, *J. Geophys. Res.* **102,** 3139–3156.

Christensen, N. I., and D. M. Fountain (1975). Constitution of the lower continental crust based on experimental studies of seismic velocities in granulite, *Geol. Soc. Am. Bull.* **86,** 227–236.

Chun, S. S., and S. K. Chough (1992). Tectonic history of Cretaceous sedimentary basins in the southwestern Korean Peninsula and Yellow Sea, in *Sedimentary Basins in the Korean Peninsula and Adjacent Seas*, S. K. Chough (Editor), Korean Sediment. Res. Group Spec. Publ., Harnlimwon Publishers, Seoul, 60–76.

Clarke, T. J., and P. G. Silver (1993). Estimation of crustal Poisson's ratio from broad band teleseismic data, *Geophys. Res. Lett.* **20,** 241–244.

Cluzel, D., B.-J. Lee, and J.-P. Cadet (1991). Indosinian dextral ductile fault system and synkinematic plutonism in the southwest of the Ogcheon belt (South Korea), *Tectonophysics* **194,** 131–151.

Ernst, W. G., and J. G. Liou (1995). Contrasting plate-tectonic styles of the Qinling-Dabie-Sulu and Franciscan metamorphic belts, *Geology* **23,** 353–356.

Fountain, D. M., and N. I. Christensen (1989). Composition of the continental crust and upper mantle: a review, in *Geophysical Framework of the Continental United States*, L. C. Pakiser and W. D. Mooney (Editors), Geol. Soc. Am. Memoir, Vol. 172, 711–742.

Hetland, E. A., F. T. Wu, and J. L Song (2004). Crustal structure in the Changbaishan volcanic area, China, determined by modeling receiver functions, *Tectonophysics* **386,** 157–175.

Holbrook, W. S., W. D. Mooney, and M. I. Christensen (1992). The seismic velocity structure of the deep continental crust, in *Lower Continental Crust*, D. M. Fountain, R. Arculus, and R. Kay (Editors), Elsevier, Amsterdam, 1–43.

Kern, H. (1982). P- and S-wave velocities in crustal and mantle rocks under the simultaneous action of high confining pressure and high temperature and the effect of the rock microstructure, in *High-Pressure Researches in Geoscience*, W. Schreyer (Editor), E. Schweizerbart'sche, Stuttgart, Germany, 15–45.

Kim, S. G., and S. K. Lee (2001). Moho discontinuity studies beneath the broadband stations using receiver functions in South Korea, *J. Korean Soc. Hazard Mitigation* **1,** 139–155 (in Korean).

Kwon, B. D., and S. Y. Yang (1985). A study on the crustal structure of the southern Korean peninsula through gravity analysis, *J. Korean Inst. Mining Geol.* **18,** 309–320.

Kwon, Y. W., C. W. Oh, and H. S. Kim (2003). Granulite-facies metamorphism in the Punggi area, northeastern Yeongnam massif, Korea and its tectonic implications for East Asia, *Precambrian Res.* **122,** 253–273.

Langston, C. A. (1979). Structure under Mount Rainier, Washington, inferred from teleseismic body waves, *J. Geophys. Res.* **84,** 4749–4762.

Lee, S. R., M. Cho, K.-W. Yi, and R. Stern (2000). Early Proterozoic granulites in central Korea: tectonic correlation with Chinese cratons, *J. Geol.* **108,** 729–738.

Li, Z. X. (1994). Collision between the North and South China blocks: a crustal-detachment model for suturing in the region east of the Tanlu fault, *Geology* **22,** 739–742.

Maruyama, S., Y. Isozaki, G. Kimura, and M. Terabayashi (1997). Paleogeographic maps of the Japanese Islands: plate tectonic synthesis from 750 Ma to the present, *The Island Arc* **6,** 121–142.

Owens, T. J., and G. Zandt (1997). Implications of crustal property variations for models of Tibetan plateau evolution, *Nature* **387,** 37–43.

Park, K. H., Y. Song, M. Park, S. Lee, and H. Ryoo (2000). Petrological, geochemical and geochronological studies of Precambrian basement in northeast Asia region. 1. Age of the metamorphism of Jirisan area, *J. Petrol. Soc. Korea* **9,** 29–39 (in Korean with English abstract).

Poirier, J. P. (1987). On Poisson's ratio and composition of the Earth's lower mantle, *Phys. Earth Planet. Interiors* **46,** 357–368.

Ree, J.-H., M. Cho, S.-T. Kwon, and E. Nakamura (1996). Possible eastward extension of Chinese collision belt in South Korea: the Imjingang belt, *Geology* **24,** 1071–1074.

Sagong, H., S.-T. Kwon, and J.-H. Ree (2005). Mesozoic episodic magmatism in South Korea and its tectonic implication, *Tectonics* **24,** TC5002, doi 10.1029/2004TC001720.

Tarkov, A. P., and V. V. Vavakin (1982). Poisson's ratio behavior in various crystalline rocks: application to the study of the Earth's interior, *Phys. Earth Planet. Interiors* **29,** 24–29.

Yin, A., and S. Nie (1993). An indentation model for the North and South China collision and the development of the Tan-Lu and Honam fault systems, eastern Asia, *Tectonics* **12,** 801–813.

Zandt, G., and C. J. Ammon (1995). Continental crust composition constrained by measurements of crustal Poisson's ratio, *Nature* **374,** 152–154.

Zandt, G., S. C. Myers, and T. C. Wallace (1995). Crust and mantle structure across the Basin and Range Colorado Plateau boundary at 37°N latitude and implications for Cenozoic extensional mechanism, *J. Geophys. Res.* **100,** 10,529–10,548.

Zandt, G., A. A. Velasco, and S. L. Beck (1994). Composition and thickness of the southern Altiplano, Bolivia, *Geology* **22,** 1003–1006.

Zhu, L., and H. Kanamori (2000). Moho depth variation in southern California from teleseismic receiver functions, *J. Geophys. Res.* **105,** 2969–2980.

School of Earth and Environmental Sciences
Seoul National University
Seoul 151-747, South Korea
joshua@snu.ac.kr
baagce@snu.ac.kr

Manuscript received 31 December 2005.